Available online at www.sciencedirect.com
SCIENCE DIRECT®
ELSEVIER
European Journal of Mechanics B/Fluids 23 (2004) 303–318
EUROPEAN JOURNAL OF MECHANICS B/FLUIDS

Skin friction and turbulence measurements in a boundary layer with zero-pressure-gradient under the influence of high intensity free-stream turbulence

B. Stefes *, H.-H. Fernholz

Hermann-Föttinger-Institut für Strömungsmechanik, Technische Universität Berlin, Strasse des 17. Juni 135, 10623 Berlin, Germany

Received 22 January 2003; accepted 22 August 2003

Abstract

This experimental investigation deals with the influence of turbulence intensities $Tu_\delta \leqslant 13\%$ and a ratio of integral length scale Λ_{11} to boundary layer thickness $\delta_{99.5}$ smaller than two on an axisymmetric turbulent boundary layer with zero pressure gradient. The free-stream turbulence was generated by jets injected normal to the flow upstream of the test section. The boundary layer had a Reynolds number range $1000 \leqslant Re_{\delta_2} \leqslant 2700$. Skin-friction measurements were performed using oil-film interferometry, Preston tubes and wall hot-wire probes. Mean and fluctuating velocities were measured by hot-wire anemometry and Reynolds stresses, triple correlations and spectra were evaluated. The free-stream turbulence increases the skin friction by up to 34% and considerably changes both mean and fluctuating velocity distributions in the outer region of the boundary layer.

Keywords: Turbulent boundary layer; Skin friction; High free-stream turbulence

1. Introduction

Free-stream turbulence (FST) is an important boundary condition for boundary layers in that it can accelerate transition in laminar boundary layers (e.g., Roach and Brierly [1]) or that it can reduce or even eliminate closed reverse-flow regions in a separated turbulent boundary layer (e.g., Kalter and Fernholz [2]). Besides changes in the turbulence structure of the boundary layer one of the most important effects of FST is the increase in skin friction and heat transfer.

The influence of free-stream turbulence on zero-pressure gradient turbulent boundary layers has been investigated in detail by Hancock and Bradshaw [3,4] and Blair [5,6], among others, for free-stream turbulence levels $Tu_\delta \leqslant 7\%$ and by Thole and Bogard [7,8] for $Tu_\delta \leqslant 20\%$. Free-stream turbulence levels up to 7% are generated in general by bar grids. They disturb the main stream but flow uniformity in the test section occurs within a reasonable distance downstream without too large a loss of the FST level. For higher FST levels, as occur for example in gas turbines, much stronger turbulence generators are necessary (for a survey see Thole et al. [9]). One such device (e.g., Thole and Bogard [8]) uses air jets normal to the mainstream flow. The turbulence level can be set by controlling the jet momentum. The disadvantage of this method is that the resulting main stream flow is highly non-uniform. It is therefore essential to strike the correct balance between the flow uniformity which increases in the downstream direction and the FST which decays.

Earlier investigations have shown that the effect of FST depends significantly on both the free-stream intensity and a length scale ratio, for example the u-component streamwise integral length scale Λ_{11} (see Section 3.2) and the boundary-layer thickness $\delta_{99.5}$. The effects of FST on the boundary layer were found to be strong, if the ratio $\Lambda_{11}/\delta_{99.5}$ is about one (Hancock

* Corresponding author.
E-mail address: stefes@bossix.pi.tu-berlin.de (B. Stefes).

0997-7546/$ – see front matter
doi:10.1016/j.euromechflu.2003.08.005

and Bradshaw [3]). The results in the present paper are designed to show the effects of varying the free-stream turbulence level $Tu_\delta = (\overline{u'^2})_\delta^{1/2}/U_\delta$ when $\Lambda_{11}/\delta_{99.5}$ is close to one. The ratio of the boundary-layer thickness $\delta_{99.5}$ to the radius of the test section corresponding to $Re_{\delta_2} \approx 2000$ was 0.13 for $Tu_\delta = 0.8\%$ and 0.31 for $Tu_\delta = 12.9\%$. It is unlikely that curvature effects play a role, since agreement of mean velocity profiles and skin friction with the data of Hancock and Bradshaw [3] in a turbulent boundary layer with free-stream turbulence on a plane wall is good. As for high free-stream data the tendency of our measurements agrees with those of Thole and Bogard [8].

This experiment aims at investigating the influence of FST levels $Tu_\delta \leqslant 13\%$ on a zero-pressure-gradient boundary layer which also provides the initial conditions for a highly-accelerated boundary layer (to be described in a subsequent paper). It complements the investigation of Thole and Bogard [8] by providing measurements in the immediate vicinity of the wall ($y^+ \approx 2$), at higher Reynolds numbers, and of skin friction. The latter data were obtained by three different techniques: oil-film interferometry, the wall hot wire and the Preston tube. This allowed estimation of accuracy of these techniques and confirmation of the logarithmic law at high FST (see Fig. 9). The experimental results are presented in the scaling used for a canonical boundary layer at low FST levels and are therefore easy to compare with the data presented by Fernholz and Finley [10], for example.

2. Experimental facility and measuring techniques

The experiments were performed in the low-turbulence wind tunnel of the Hermann-Föttinger-Institut. The wind tunnel is a closed return facility with a centrifugal fan and a 15 kW motor and an additional 1 kW blower to remove the nozzle boundary layer at the start of the test section (for details see Fernholz and Warnack [11]). The axisymmetric test section (6 m length) consisted of Perspex pipe sections (0.44 m inner diameter) of various lengths, one of which had an elliptical leading edge (6:1) and determined the origin of the test boundary layer on the wall of the test section. The air temperature was kept constant within $\pm 0.1°$C. The velocity in the test section was below or equal to 10 m/s and could be controlled to 0.3%.

The turbulence generator was situated between the nozzle exit and the test section and consisted of a cylindrical pipe section the wall of which had holes to inject the air jets normal to the mainstream. The air supply for the jets was provided from a circular settling chamber (Fig. 1) and the velocity at the jet nozzle exit was uniform within $\pm 1.5\%$ around the circumference. The diameter D of the jet holes was 20 mm and their centres were 3D apart around the circumference, as suggested by Thole and Bogard [8]. A perforated metal cylinder along the centerline of the turbulence generator and an adjacent perforated metal cone served to smoothen the jet interaction and the mean velocity distribution. For the generation of the FST the ratio of jet to mainstream velocity was varied between 0 and 6.3, generating FST levels of approximately 0.8% (case 10), 5% (case 20),

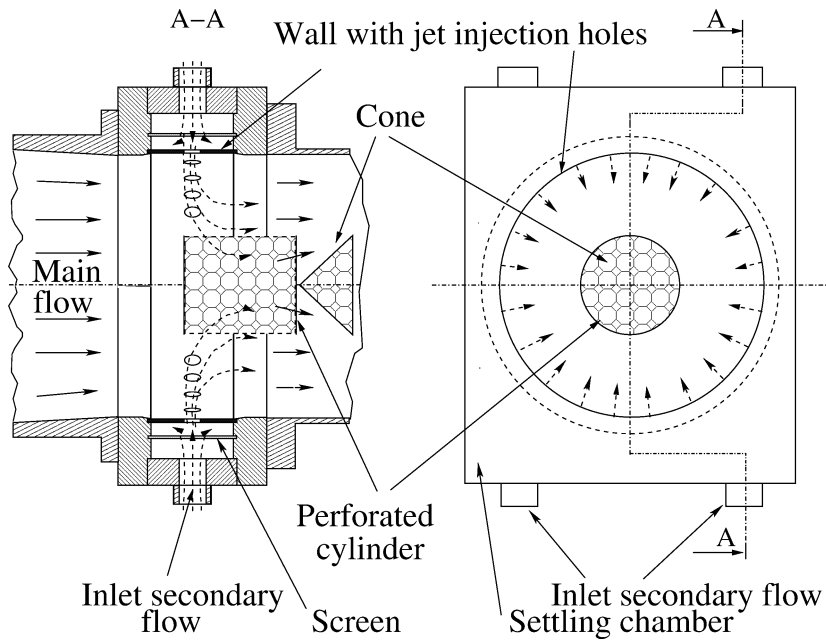

Fig. 1. Turbulence generator upstream of the test-section inlet.

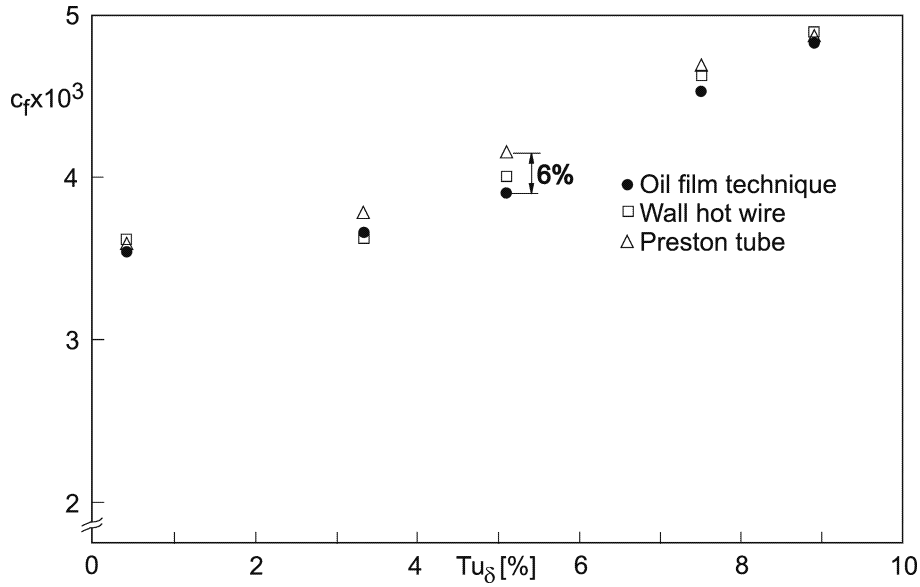

Fig. 2. Comparison of skin-friction measured in a ZPG boundary layer with various FST levels by three different techniques ($1200 \leqslant Re_{\delta_2} \leqslant 2700$).

11% (case 30), and 13% (case 40), where 0 in the case numbering denotes ZPG. The downstream end of the turbulence generator was 265 mm upstream of the leading edge of the test wall ($x = 0$).

Mean and fluctuating components of the velocity were measured using miniature single and X-wire probes with the stem (3 mm diameter) protruding through plugs in the test wall. The prongs of the crossed-wire probe were mounted at the corners of a square of side length 1.5 mm and the tungsten/platinum wires, gold plated at the ends, had an active length of 0.55 mm and a diameter of 2.5 μm.

The constant-temperature hot-wire anemometer was an IFA 100 from TSI and data acquisition was achieved using a PC with a 16 bit A/D converter on a data acquisition board. The probes were traversed using an electrically driven traverse gear with an incremental resolution of 0.001 mm. Probe access was through an interchangeable plug in the wall of the test section. 524 K samples (at a frequency of 20 kHz) were taken for all velocity measurements. For the wall hot wire the sampling frequency was 20 kHz (1048 K samples).

Skin friction was measured by means of Preston tubes (diameter between 2 and 4 mm), wall hot-wire probes and by oil-film interferometry. The two probes were each integrated into one of the interchangeable plugs in the test wall (see Fernholz and Warnack [11] for details). The wall hot-wires were 0.090 mm away from the wall ($y^+ \approx 2$) and they were calibrated by means of the Preston tube at low Tu_δ with the Patel [12] calibration curve. Details of the oil-film interferometry method were given by Fernholz et al. [13], for example. Fig. 2 provides the comparison of the three methods. The skin friction $\bar{\tau}_w$ was made dimensionless with $\rho_\delta U_\delta^2$ at the measuring station ($x = 1.552$ m) and the skin friction coefficient $c_f = 2\bar{\tau}_w/\rho_\delta U_\delta^2$ was plotted against Tu_δ.

If one accepts that the determination of the skin friction by the oil-film interferometry lies within an error band of ±4% then the wall hot wire data fall within this range and the Preston tube measurements are slightly higher. This can be explained by the nonlinear behaviour of the Preston tube which was calibrated originally in a boundary layer with low FST (Patel [12]) and is used here under the influence of high FST where the turbulence structure changes, e.g., the skewness and flatness of the fluctuating skin friction are higher (Fig. 16). For these measurements, the Reynolds number Re_{δ_2} varied between 1200 and 2700.

The turbulence generator was optimized to achieve an approximately uniform distribution of the fluctuating velocity u' in a region between 50 and 100 mm normal to the wall (see Fig. 3) which determined the free-stream turbulence level for the boundary layer. In the centre region of the test section the mean velocity distributions show a wake-like behaviour and the fluctuating velocities a plateau for cases 10 and 20 and almost uniform distributions for cases 30 and 40 (Fig. 3) (for details see Stefes [14]). Both wakes and plateaus level off in downstream direction. Fig. 4 shows the decay of Tu_δ at a height $y = 75$ mm above the test wall for the four cases and for one bar-grid case for comparison. The first boundary layer profile was measured at $x = 0.828$ m where the turbulence is already decaying according to the usual exponential law with exponents n between

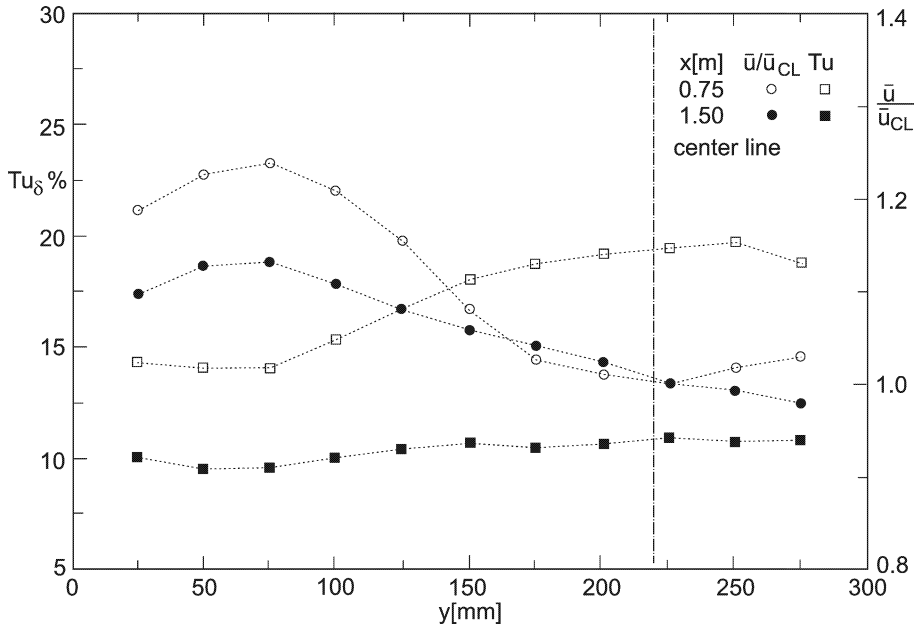

Fig. 3. Distributions of the mean velocity and the turbulence intensity in wall-normal direction at two stations in streamwise direction for a high FST level (case 40).

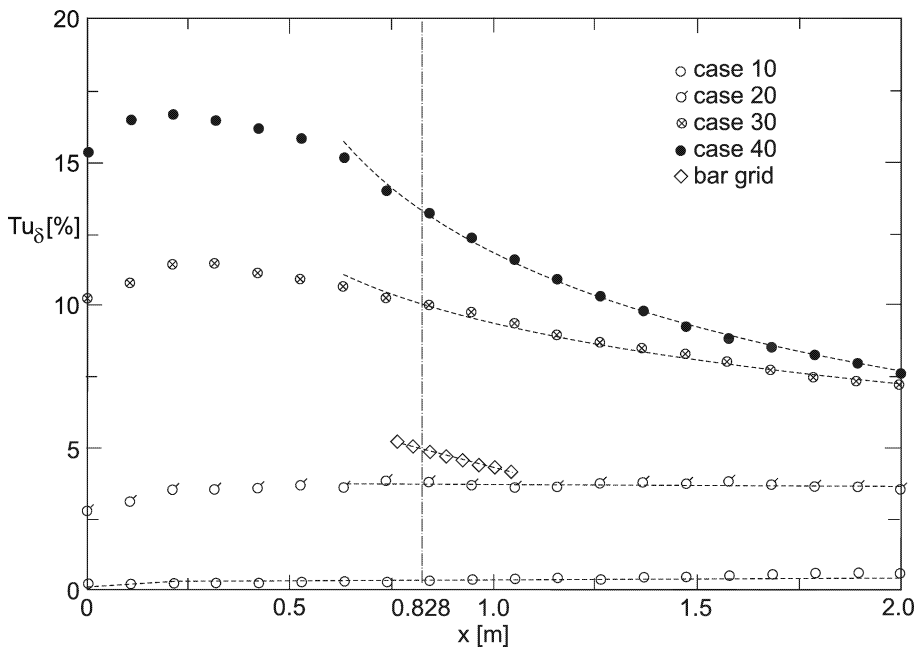

Fig. 4. Decay of free-stream turbulence level for the four cases in streamwise direction at $y = 75$ mm above the test wall (lines are for visual aid only).

-0.63 and $+0.22$ (no free-stream turbulence). It should be noted that bar-grid generated turbulence has a faster decay rate in streamwise direction ($n = -0.74$) than the comparable turbulence generated by the present turbulence generator.

Earlier investigations have shown that the effect of the FST depends both on the free-stream intensity and a length scale of the turbulence in relation to the boundary layer thickness $\delta_{99.5}$. As found by Hancock and Bradshaw [3] this ratio should be near one if an integral length scale is chosen, for example, the u-component streamwise integral length scale Λ_{11} (see

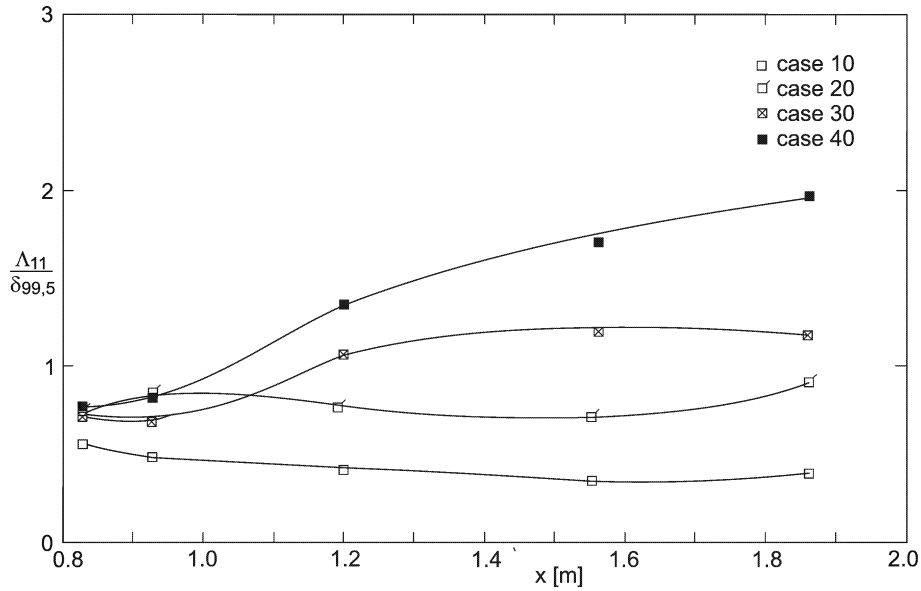

Fig. 5. Streamwise distribution of the integral length scale ratio $\Lambda_{11}/\delta_{99.5}$ for the four cases 10 to 40 along the test wall at $\delta_{99.5}$.

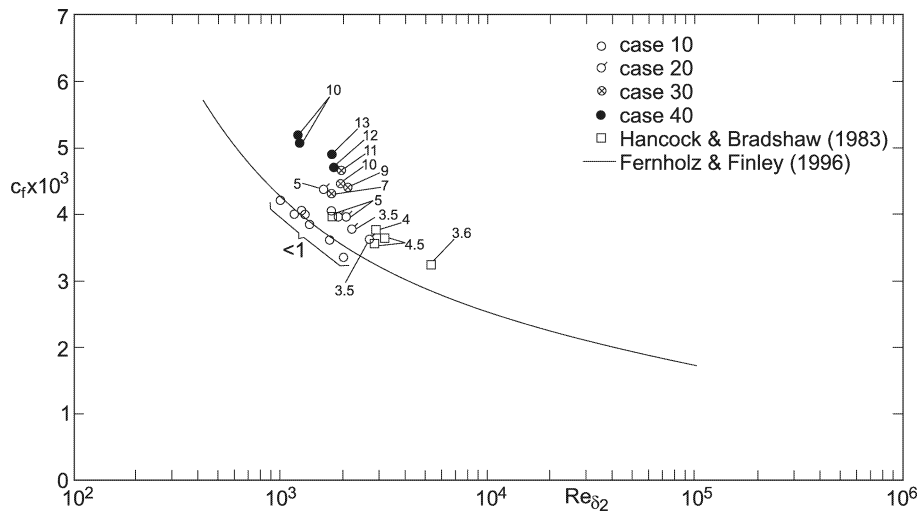

Fig. 6. Variation of skin-friction coefficient with Reynolds number and free-stream turbulence level Tu_δ (numbers denote Tu_δ %).

Section 3.2). This was calculated from the measured autocorrelations and the distributions in streamwise direction for the four cases are shown in Fig. 5. At the higher turbulence levels (cases 30 and 40) the length-scale ratio increases in the downstream direction because Λ_{11} increases and $\delta_{99.5}$ decreases due to the falling FST level. This increase from $\Lambda_{11}/\delta_{99.5}$ near one to at most two may slightly affect both c_f and H_{12} but the present measuring methods do not allow a final statement (see Figs. 6 and 7). It should be noted that Λ_{11} was much larger for the high turbulence cases than for the low FST cases (see also Thole and Bogard [8]). Profiles of Λ_{11} and Λ_{12} as a function of y/Δ are presented later in this paper. For a comparison with the investigations of Hancock and Bradshaw [3] and of Castro [15] values of their length scale of the free-stream turbulence L_e^u are quoted. In cases 30 and 40 $L_e^u/\delta_{99.5}$, as calculated from the measurements, fell in the range between 1.2 and 2.8, rising in the downstream direction. This is in agreement with the values given by the above authors.

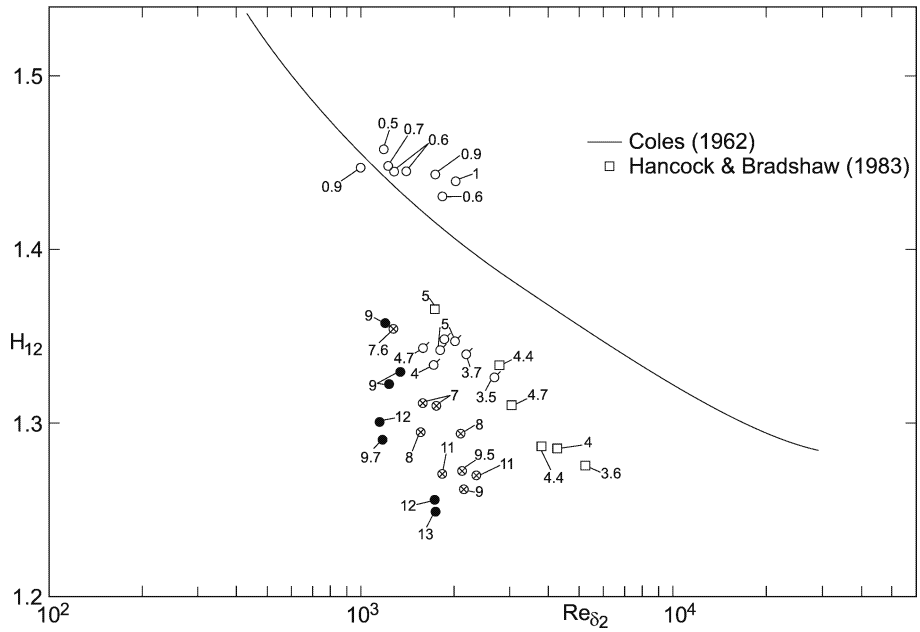

Fig. 7. Variation of shape parameter H_{12} with Reynolds number and free-stream turbulence level Tu_δ (for symbols see Fig. 9 and numbers denote Tu_δ %).

3. Discussion of the measurements

3.1. Skin-friction data and mean velocities

It is generally accepted that the skin-friction coefficient c_f in a canonical boundary layer is a function of the Reynolds number $Re_{\delta_2} = U_\delta \delta_2/\nu$ only (e.g., Fernholz and Finley [10]). In a ZPG boundary layer with FST two additional parameters must be taken into account, the FST level Tu_δ and the ratio of a characteristic length scale, e.g., $\Lambda_{11}/\delta_{99.5}$:

$$c_f = f(Re_{\delta_2}, Tu_\delta, \Lambda_{11}/\delta_{99.5}).$$

If the length scale ratio can be kept constant, preferably near one for an optimal effect on the boundary layer (Hancock and Bradshaw [3]), c_f can be plotted as a function of Re_{δ_2} with Tu_δ as the only parameter (Fig. 6). For a comparison with the data where $Tu_\delta \approx 0$, the semi-empirical relationsship of Fernholz and Finley [10] is given. At constant Re_{δ_2} the measurements show the expected increase of the skin friction with rising values of Tu_δ, reaching a value 34% higher for $Tu_\delta = 13\%$ than for $Tu_\delta \approx 0$. The increase of the skin friction $\bar{\tau}_w$ is due to the increase in the slope $(\delta\bar{u}/\delta y)_w$ caused by the fuller mean velocity profile. This again is reflected in lower values of the shape parameter $H_{12} = \delta_1/\delta_2$ (where δ_1 denotes the displacement thickness). The boundary layer thicknesses δ_1 and δ_2 were calculated with consideration of the radius of curvature of the test wall (for the definitions see Fernholz and Warnack [11]). Fig. 7 presents the relationship $H_{12} = f(Re_{\delta_2})$ for $Tu_\delta \approx 0$ given by Coles [16] in comparison with measurements of H_{12} at different values of the FST level. Measurements from a boundary layer with bar-grid generated turbulence ($Tu_\delta \approx 4\%$) complement our data well (Hancock and Bradshaw [3]), showing that the generation mechanism of the FST produces a similar turbulence structure, at least at low levels of the turbulence intensity.

In order to compare the present results more easily with the earlier measurements of Hancock and Bradshaw [3] as well as Blair [6] and Castro [15] the fractional increase in skin friction $\Delta c_f/c_{f_0}$ was plotted against the empirical combined length-scale-intensity variable (Blair [6]) $\mathrm{HBB} = Tu_\delta/[(L_e^u/\delta_{99.5}+2)(1+3\cdot\exp(-Re_{\delta_2}/400))]$. Fig. 8 shows that there is a reasonable correlation between the increase in skin friction and the HBB parameter with a plateau beginning at about $\mathrm{HBB} = 3$ which is, however, lower than that shown by Bott and Bradshaw [17].

The mean velocity profiles are presented in inner- and outer-law scaling where the velocity was obtained by a single normal hot-wire probe and the skin friction by a wall hot-wire probe. From among the 24 velocity distributions measured, four with Reynolds numbers $Re_{\delta_2} \approx 1800$ were chosen for a comparison. Their FST level Tu_δ varied between 1% and 13%. Fig. 9 shows the measurements in inner-law scaling with the linear law

$$u^+ = \frac{\bar{u}}{u_\tau} = \frac{y u_\tau}{\nu} = y^+ \tag{1}$$

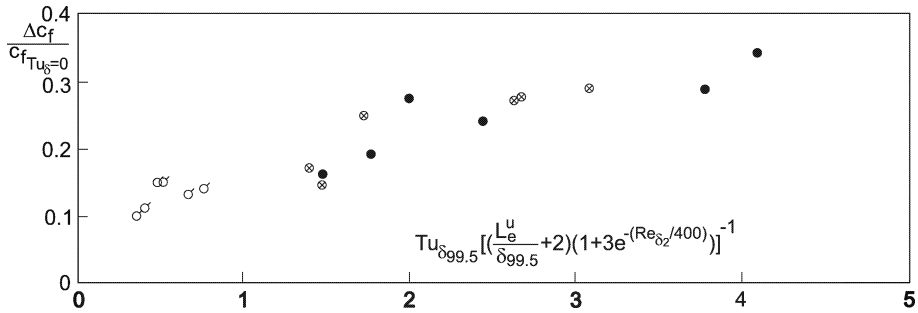

Fig. 8. Fractional increase in skin-friction coefficient against Hancock–Bradshaw–Blair parameter (HBB).

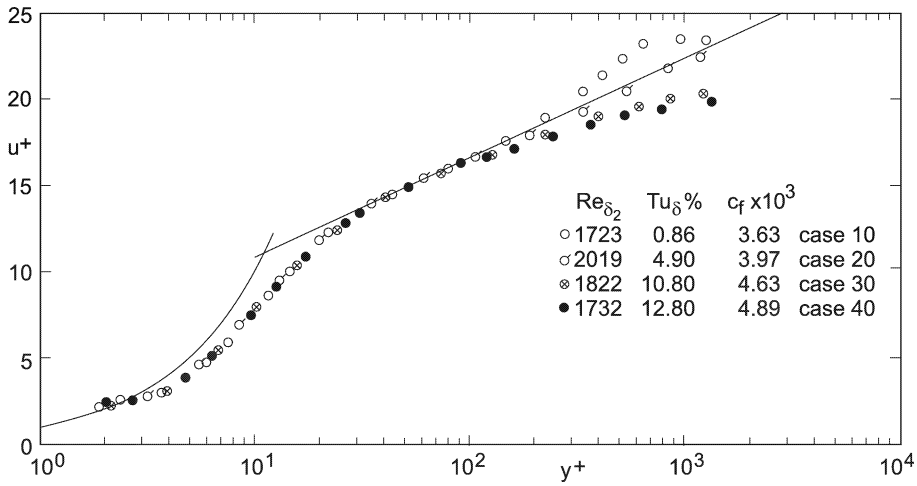

Fig. 9. Mean velocity profiles in inner-law scaling at various free-stream turbulence levels.

and the logarithmic law

$$u^+ = (1/\kappa)\ln y^+ + C. \tag{2}$$

Here $u_\tau = \sqrt{\tau_w/\rho}$ is the skin friction velocity and the constants were chosen as $\kappa = 0.40$ and $C = 5.10$. The mean velocity profiles (Fig. 9) agree well with the log law over a distance which decreases in length with rising Tu_δ. The main effect of the FST is, however, on the outer layer wake component (see Castro [15]) for comparison), and on the outer-law distribution (Fig. 10). The outer-law velocity distribution has the following form

$$\frac{u_\delta - \bar{u}}{u_\tau} = f\left(\frac{y}{\delta}, \frac{L}{\delta}, \frac{(u'_{\mathrm{rms}})_\delta}{u_\tau}, \frac{u_\delta}{u_\tau}\right) \tag{3}$$

which can be simplified according to Rotta [23] to

$$\frac{u_\delta - \bar{u}}{u_\tau} = f\left(\frac{y}{\Delta}, \frac{\Lambda_{11}}{\delta}, Tu_\delta\right) \quad \text{with } \Delta = \int_0^\delta \frac{u_\delta - \bar{u}}{u_\tau}\,\mathrm{d}y. \tag{4}$$

Plotted in this outer-law scaling the deviations from the velocity profile with small FST represented by the straight line (see Fernholz and Finley [10]), are large. Thole and Bogard [8] observed a collapse of the defect velocity profiles for FST levels above 12% which indicates a constant wake strength. This behaviour can also be anticipated from the present data. In outer-law scaling the mean velocity profiles show similar behaviour to those in a favourable pressure gradient (cf. Fernholz and Finley [18], their Fig. 5.2.2). In both cases the boundary conditions – although quite different – generate velocity profiles which are fuller than in a canonical boundary layer.

Three components of the Reynolds stress tensor were measured, $\overline{u'^2}$, $\overline{v'^2}$ and $\overline{u'v'}$. Scaled with u_τ^2 they are presented in inner-law scaling in Figs. 11–13. The Reynolds normal stress component $\overline{u'^2}/u_\tau^2$ is shown in Fig. 11. There is a certain degree

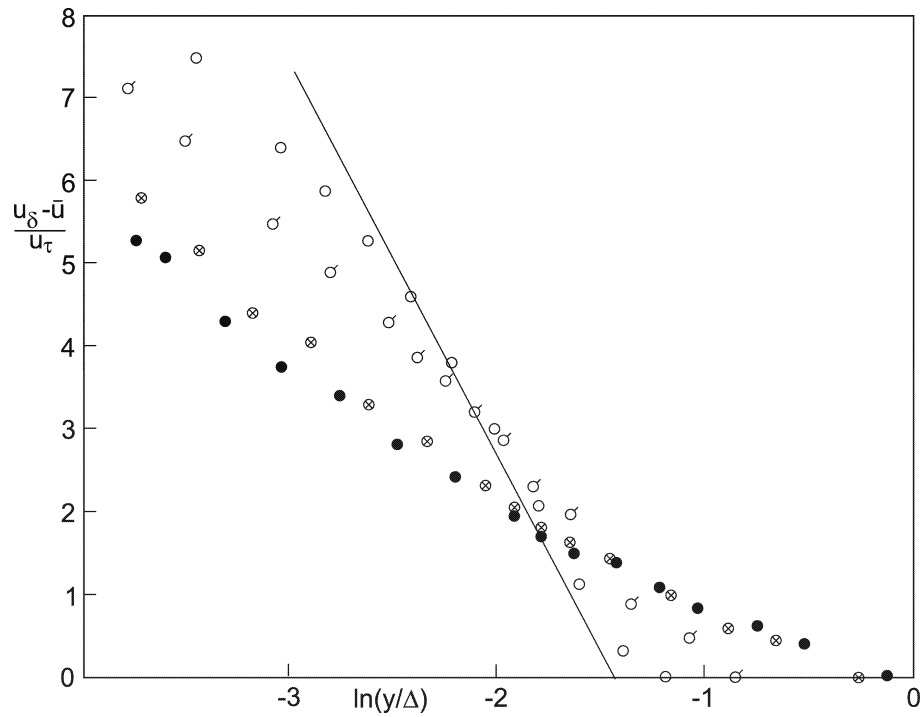

Fig. 10. Mean velocity profiles in outer-law scaling at various free-stream turbulence levels (for symbols see Fig. 9).

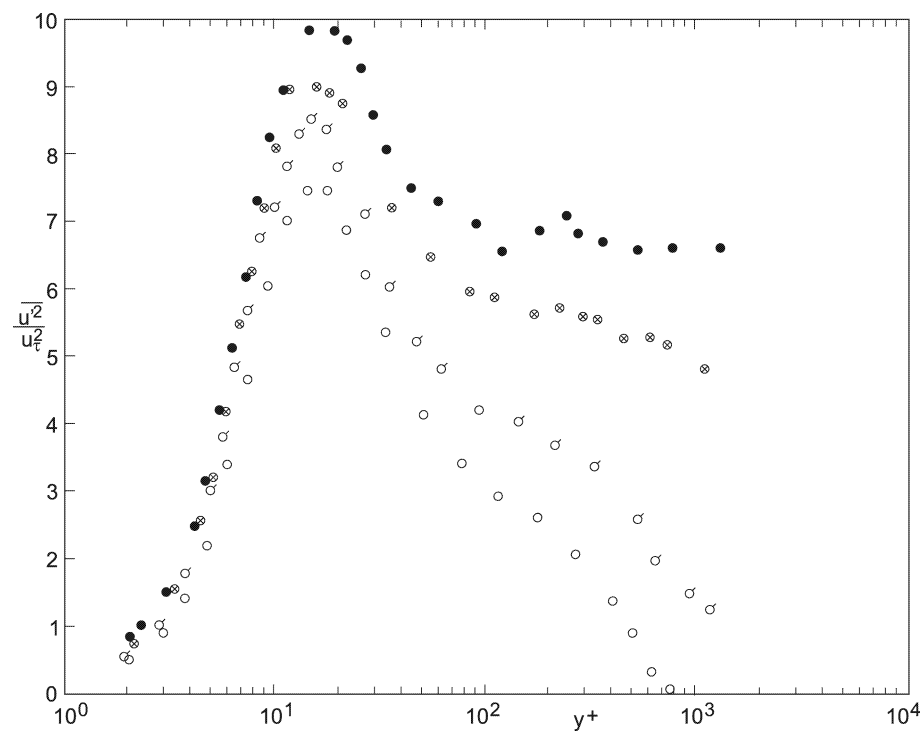

Fig. 11. Profiles of Reynolds normal-stress component $\bar{\rho}\overline{u'^2}$ in inner-law scaling for various free-stream turbulence levels (for symbols see Fig. 9).

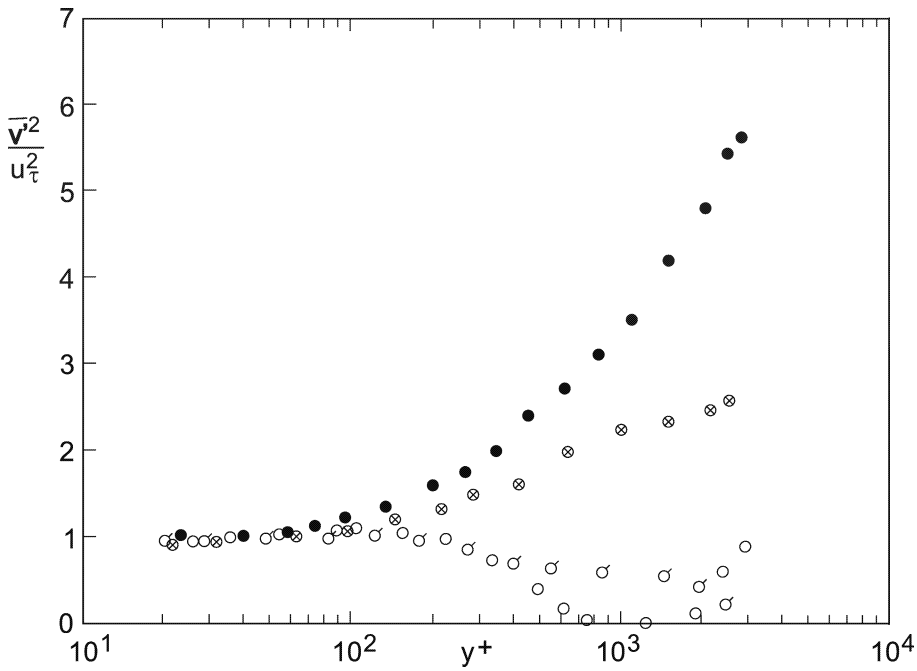

Fig. 12. Profiles of Reynolds normal-stress component $\bar{\rho}\overline{v'^2}$ in inner-law scaling for various free-stream turbulence levels (for symbols see Fig. 9).

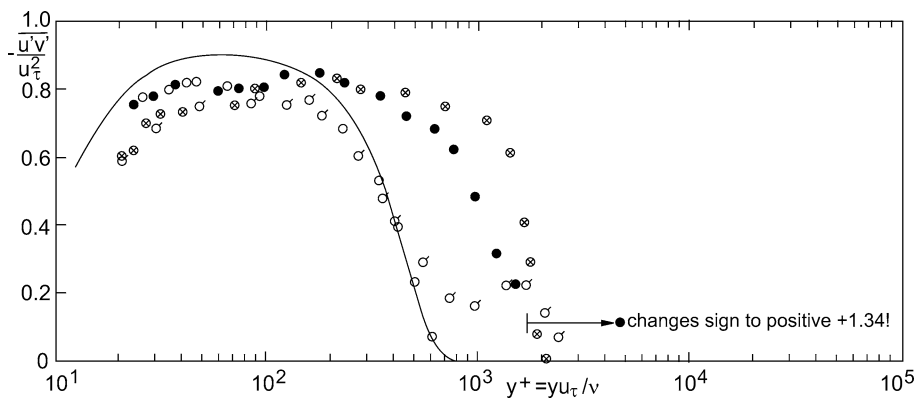

Fig. 13. Profiles of Reynolds shear-stress $\bar{\rho}\overline{u'v'}$ in inner-law scaling for various free-stream turbulence levels (for symbols see Fig. 9). The line denotes data of Spalart [20] for $Re_\theta = 1410$.

of self-similarity in the linear region and the buffer layer ($y^+ < 10$), and an increase of the maximum value with rising Tu_δ. The location of the maximum value differs very little from that of a low FST-level profile at $y^+ \approx 15$. The value of $(\overline{u'^2}/u_\tau^2)_{\max}$ increases by about 25% for $Tu_\delta = 13\%$ as compared with $Tu_\delta = 1\%$ and this must be attributed to the intrusion of the FST into the boundary layer since the Reynolds number Re_{δ_2} is approximately constant. As already noted by Thole and Bogard [8] the distribution of $\overline{v'^2}/u_\tau^2$ is completely different from the $\overline{u'^2}/u_\tau^2$ profiles (Fig. 12). In the near-wall region all profiles collapse on one curve, a behaviour which is certainly due to the defects of the X-wire measurements (see also Österlund and Johansson [19]). $\overline{v'^2}$ must of course tend to zero at the wall as is clear from LDA-measurements. A comparison of the $\overline{u'^2}$- and $\overline{v'^2}$-distributions shows that their ratio is about 0.8 in the outer layer. Fig. 13 presents the corresponding Reynolds shear-stress profiles which confirm the observation of Hancock and Bradshaw [3] that the Reynolds shear stress approaches zero before the $\overline{v'^2}$ components reach their free-stream value. The profiles for the cases with the higher FST extend further out into the outer layer than those with low FST showing the strong effect of the FST. The maximum value of case 10 can be compared with the numerical calculations of Spalart [20]. The DNS calculations show a maximum value about 9% higher but well below unity.

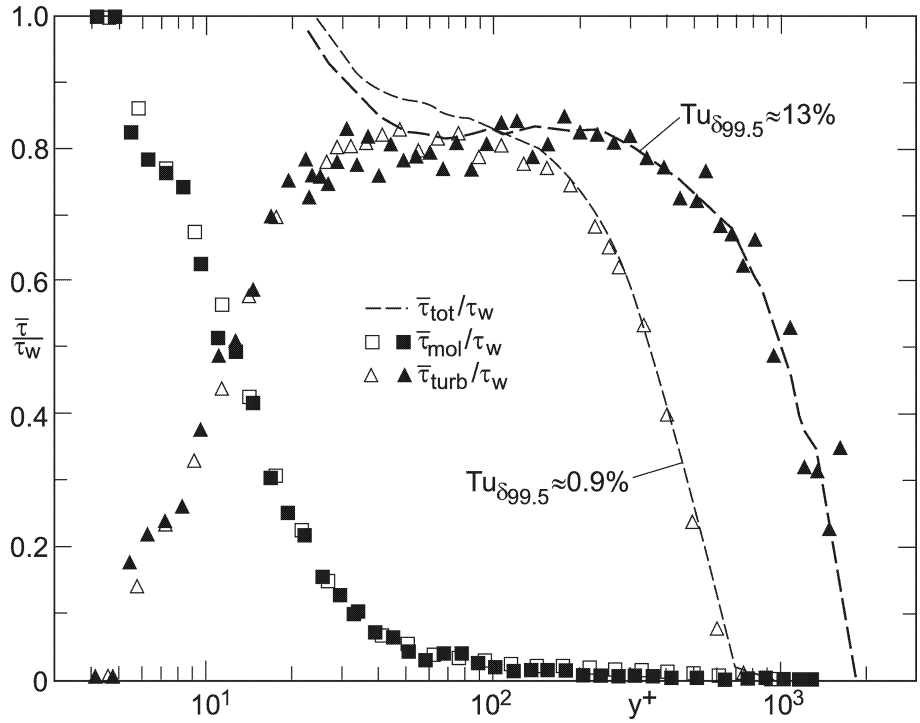

Fig. 14. Shear-stress profiles (measured and calculated) in inner-law scaling at $Re_{\delta_2} = 1728$ and two free-stream turbulence levels (Reynolds shear-stress calculated below $y^+ \approx 25$).

The departure of the maximum value of the dimensionless Reynolds shear stress from unity is a low Reynolds number effect as shown by Fernholz and Finley [10] from a comparison with measurements of various authors (see Fernholz and Finley [10], their Figs. 24, 25 and 57). A further comparison with LDV measurements was given by Karlsson and Johansson [21].

In order to obtain the Reynolds shear stress distribution nearer to the wall the total shear stress was calculated from the measured viscous and Reynolds shear stress: Once τ_{tot}/u_τ^2 had reached one it remains constant down to the wall and can now be used to calculate $\rho\overline{u'v'}$ by deducting the viscous shear stress $\mu\delta\bar{u}/\delta y$ determined from the measured mean velocity profile – from the total shear stress. The measured and the calculated shear stress distributions for two profiles with various FST are shown in Fig. 14. The location at which the viscous and the Reynolds shear stress are equal is approximately at the location where $\overline{u'^2}/u_\tau^2$ has its maximum (cf. Fig. 11). The calculated distribution of the Reynolds shear stress will be used below to determine the turbulence production.

Fig. 15 shows profiles of the skewness $S_{u'} = \overline{u'^3}/(\overline{u'^2})^{3/2}$ and the flatness $F_{u'} = \overline{u'^4}/(\overline{u'^2})^2$. The skewness was found to be independent of Re_{δ_2} for low values of Tu_δ (see Fernholz and Finley [10] their Fig. 66) and it is evident that there is only a small effect of Tu_δ on $S_{u'}$ in the immediate vicinity of the wall and the log-law region. No effect of Reynolds number or FST on the flatness can be observed in the log-law region ($F_{u'} \approx 2.8$) but the near-wall region is affected, with higher values for cases 30 and 40. This means that the frequency of events far from the axis increases with rising free-stream turbulence. The usual high values of $F_{u'}$ at the edge of a boundary layer with low FST (case 10) are absent in the other three cases due to the strong mixing process caused by the high level of the FST (see also Kalter and Fernholz [2]).

The observation of Ueda and Hinze [22] that the y^+ positions of the maximum of $\overline{u'^2}$, the minimum of $F_{u'}$ and the zero value of $S_{u'}$ coincide holds also in cases where the FST level is high (see also Fernholz and Finley [10]).

The effects of the FST on the values of the fluctuating skin-friction coefficient $c'_f = 2\tau'_{rms}/(\rho_\delta U_\delta^2)$ and its higher moments $S_{\tau'_w}$ and $F_{\tau'_w}$ are displayed in Fig. 16. c'_f increases from about 1.3×10^{-3} at low FST to about 2×10^{-3} at $Tu_\delta \approx 13\%$. Such an increase with Tu_δ is also evident for $S_{\tau'_w}$ and $F_{\tau'_w}$ confirming what was found from the $S_{u'}$- and $F_{u'}$-profiles in Fig. 15. One of the more important diffusion terms in the transport equation for the turbulent energy is $\delta(\overline{u'^2v'})/\delta y$ which should be affected by the FST since the term $(\overline{u'^2v'})$ accounts for the transport of $\overline{u'^2}$ by the wall-normal fluctuation velocity v'. Fig. 17 shows profiles of $(\overline{u'^2v'})$ normalized with u_τ^3 plotted against y/Δ. It has been known from Fernholz and Finley [10] that there is no Reynolds number similarity for this distribution at low FST levels (their Fig. 74) but since Re_{δ_2} is practically constant for the

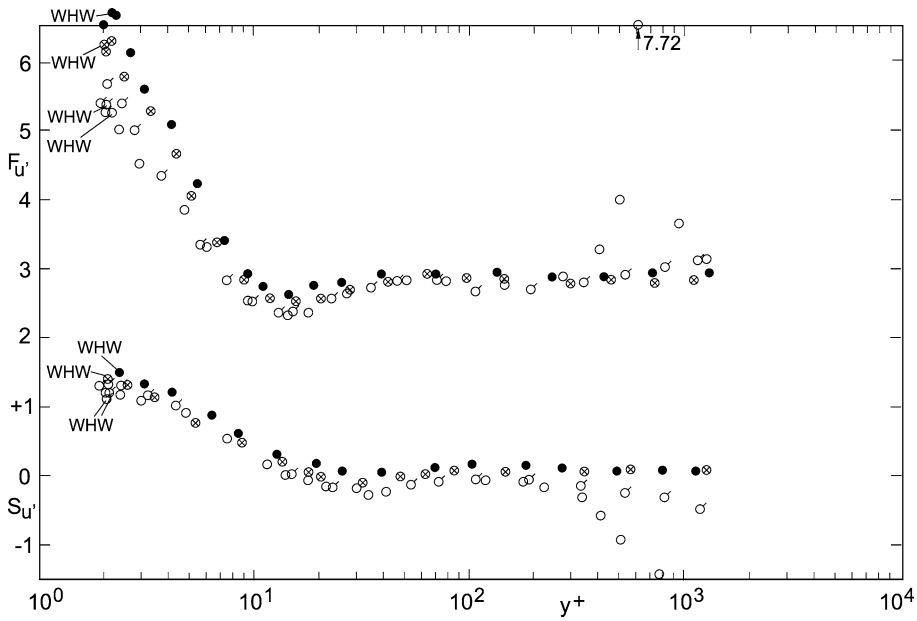

Fig. 15. Profiles of skewness $S_{u'}$ and flatness $F_{u'}$ in inner-law scaling for various free-stream turbulence levels (for symbols see Fig. 9).

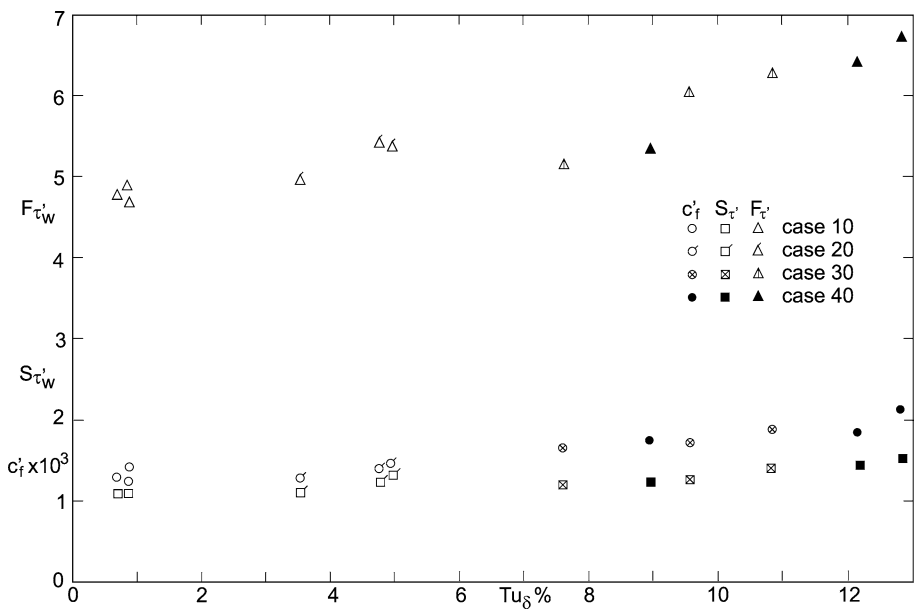

Fig. 16. Variation of fluctuating skin-friction coefficient c'_f, skewness $S_{\tau'_w}$ and flatness $F_{\tau'_w}$ with free-stream turbulence intensity Tu_δ %.

four cases shown here, deviations between the distributions must be due to the turbulence intensity. The four distributions are qualitatively similar. They show a double peak with the inner peak higher for the low turbulence case 10 (in agreement with Fernholz and Finley [10]) and the outer peak higher for the three cases with high FST ($y/\Delta = 0.2$ corresponds to roughly 0.75 $\delta_{99.5}$). This is plausible since both $\overline{u'^2}$ and $\overline{v'^2}$ have high values in the outer layer (see Figs. 11 and 12) and it can be inferred that the turbulent-transport mechanism for the kinetic turbulent energy is significantly affected by the FST in the outer region of the boundary layer. For the distributions of the diffusion term ($\overline{u'v'^2}$) in the Reynolds shear stress equation the reader is referred to Stefes [14].

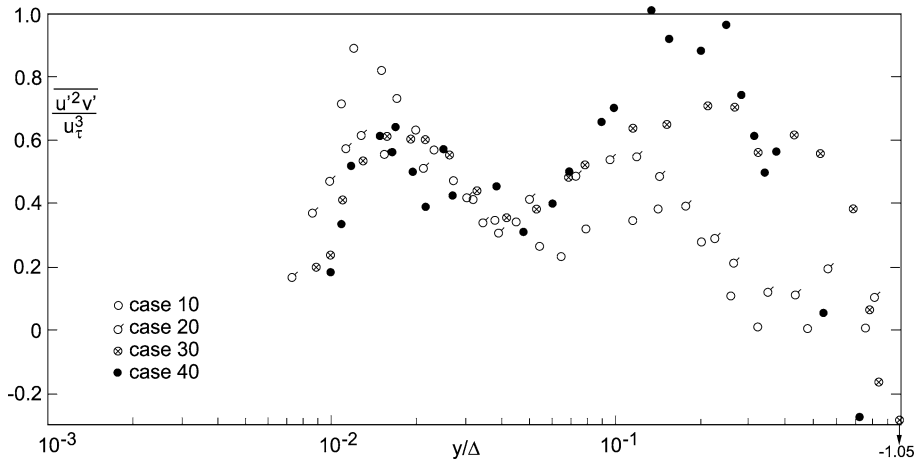

Fig. 17. Distribution of the triple correlation $\overline{u'^2v'}/u_\tau^3$ in outer-law scaling at various turbulence levels (symbols as in Fig. 9).

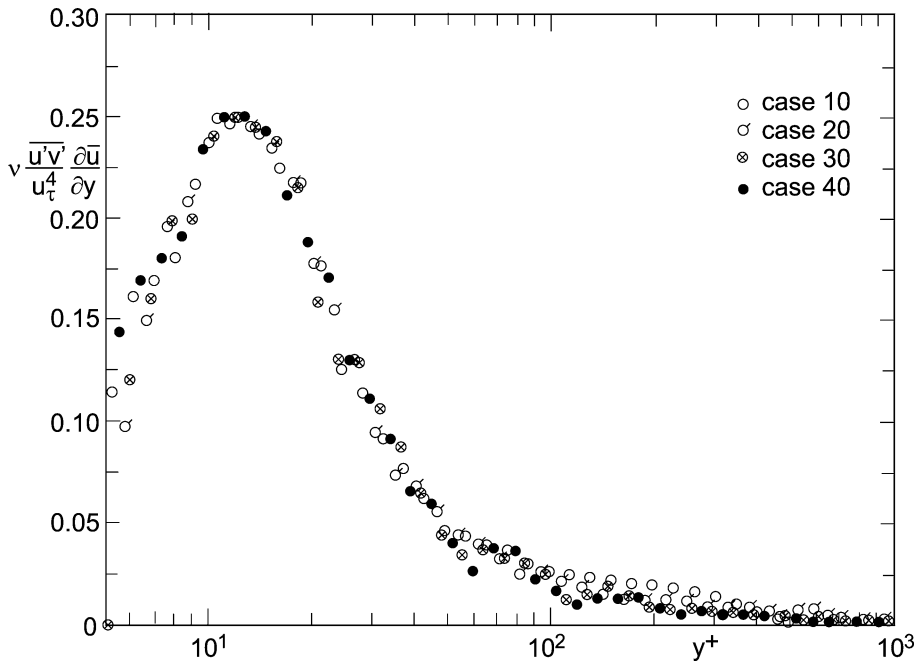

Fig. 18. Distribution of the production term for the Reynolds normal stress in inner-law scaling at various turbulence levels, calculated and measured (symbols as in Fig. 9).

Another indication of the influence of the FST is the distribution of the production of the turbulent kinetic energy $(-\overline{u'v'}\partial\bar{u}/\partial y)$. This term cannot be measured very close to the wall with a hot-wire probe but can be determined from calculated values of $(\overline{u'v'})$ as shown in Fig. 14. Measured and calculated values of the non-dimensional production term $(\nu/u_\tau^4)\overline{u'v'}\frac{\delta\bar{u}}{\delta y}$ are plotted against y^+ in Fig. 18. Rotta [23] has shown that for low FST the production term has a maximum value at 0.25 and that here the Reynolds shear stress and the viscous shear stress are equal in magnitude. In this scaling – and with the Reynolds number approximately constant – the production in the inner layer is not affected by the free-stream turbulence and its influence is confined to the outer layer. Here the production term falls with rising FST because $\partial\bar{u}/\partial y$ decreases as the result of the fuller mean velocity profiles.

3.2. Spectra and integral length scales

Since long time series were recorded from the hot-wire measurements, power spectra can be calculated at any location in the boundary layer and in the freestream. The effect of the turbulence intensity on the longitudinal wave number spectrum $E_{11}(k_1)$ is presented at a location in the log-law region ($y^+ \approx 100$) and in the freestream ($\delta_{99.5}$) at four values of Tu_δ each. The Reynolds number Re_{δ_2} for these velocity profiles was kept approximately constant. $E_{11}(k_1)$ – where $k_1 = 2\pi f/\bar{u}$ is the wavenumber – is usually scaled by $v_k^2\eta = (\varepsilon\nu^5)^{1/4}$ and plotted against $k_1\eta = k_1(\nu^3/\varepsilon)^{1/4}$. Here η denotes the Kolmogorov microscale, v_k the Kolmogorov velocity and ε the dissipation of the turbulence energy. For further details of the assumptions and the derivation of the following relationship for the dimensionless longitudinal wave-number spectrum

$$\frac{E_{11}}{v_{k_1}^2\,\eta} = F(k_1\eta, Re_\lambda) \tag{5}$$

the reader is referred, for example, to Fernholz and Warnack [11]. $Re_\lambda = \sqrt{\overline{u'^2}} \cdot \lambda/\nu$ is the turbulent Reynolds number with λ as the Taylor microscale. In this scaling two spectra are equal if Re_λ is the same.

Fig. 19 shows the power spectra in the freestream at $\delta_{99.5}$ for four different values of Tu_δ. There is the expected difference between the spectrum at low FST and those at higher FST level and a collapse of the spectra onto one curve with approximately equal turbulence Reynolds number. This and the following two figures contain dashed lines which characterize the inertial subrange of the equilibrium spectrum ($E \sim k^{-5/3}$), at higher wavenumbers ($E \sim k^{-7}$) and in the lower wave number range ($E \sim k^{-1}$). For details see, e.g., Hinze [24]. The spectrum with low FST and low Re_λ departs earlier from the $k^{-5/3}$ behaviour than the three others. Further, a comparison with the spectrum measured at low FST by Sandborn and Marshall [25] and presented in Warnack and Fernholz [26] (their Fig. 22) shows that at $Re_\lambda = 400$ the spectra with the high FST level extend to higher values showing the influence of the FST in the range of the lower frequencies.

At the beginning of the log-law region (Fig. 20) the influence of the FST is rather small. Within the range $150 \leqslant Re_\lambda \leqslant 305$ the four spectra collapse over two decades of $k_1\eta$ and differ only slightly in the low wave-number region. The agreement with the $k^{-5/3}$ law is reduced to a small range, as is to be expected, and that with k^{-1} is increased. We should note here that a direct comparison with the spectra measured by Thole and Bogard [8] is not possible since they used different scaling. In our case, spectra very close to the wall ($y^+ \approx 15$) were not presented since the Taylor hypothesis presumably does not hold because of the high turbulence level.

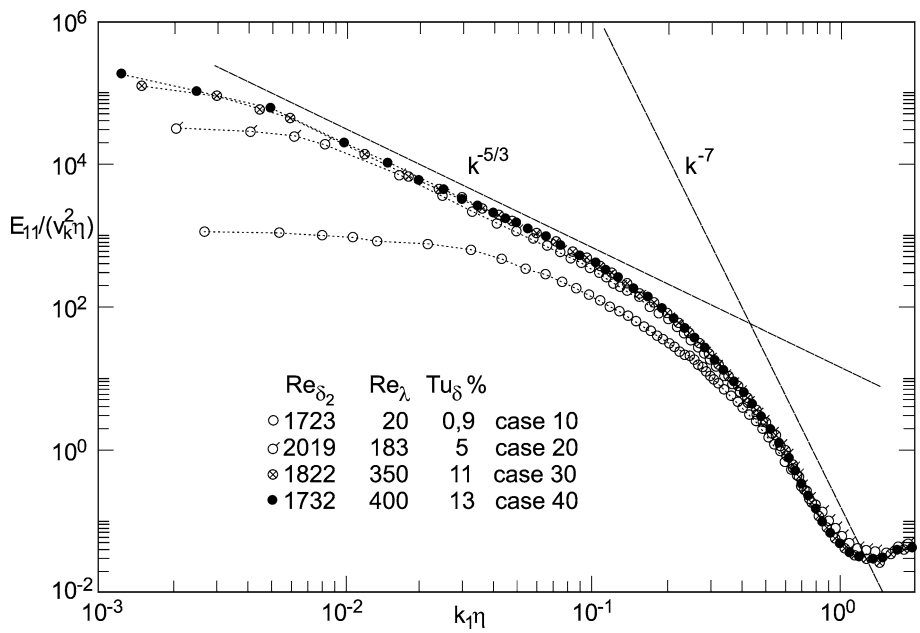

Fig. 19. One-dimensional spectra in Kolmogorov scaling at $\delta_{99.5}$ at various free-stream turbulence levels and approximately constant Re_{δ_2}.

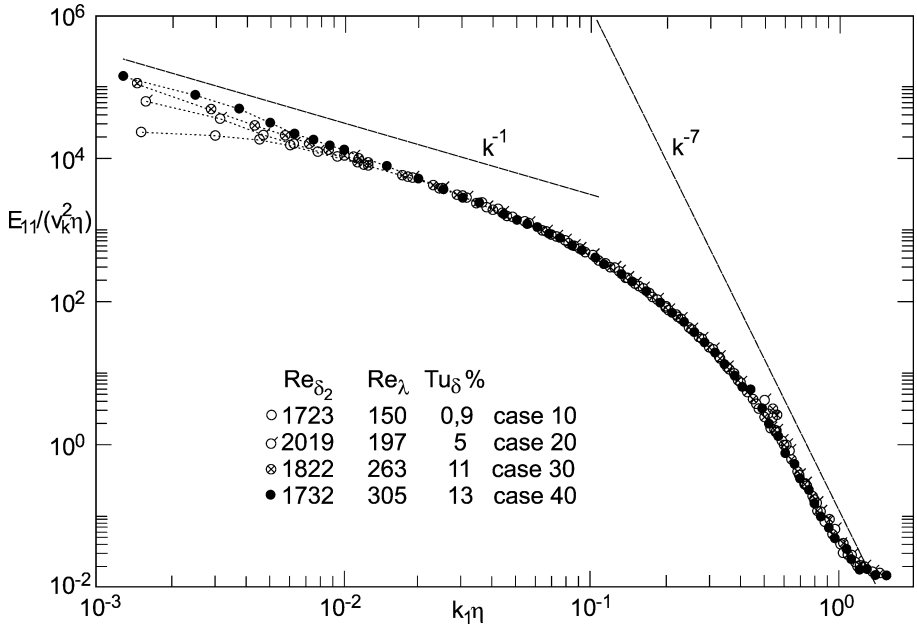

Fig. 20. One-dimensional spectra in Kolmogorov scaling at $y^+ = 100$ at various free-stream turbulence levels and approximately constant Re_{δ_2}.

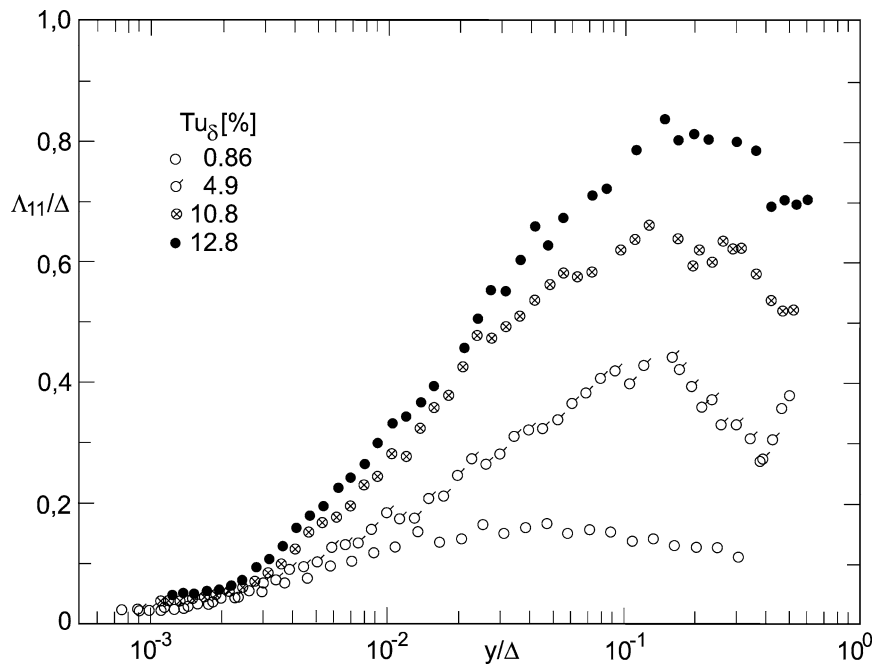

Fig. 21. Distribution of the dimensionless integral length scale Λ_{11}/Δ in outer-law scaling at various FST levels and constant Re_{δ_2}.

The behaviour of the large structures under the influence of the various levels of free-stream turbulence was investigated by measuring the autocorrelation R_τ and the space correlation of u' in the wall normal direction $R^{\Delta y}_{u'u'}$. These quantities were used to determine the integral length scales in the boundary layer

$$\Lambda_\tau = \int_0^\tau R_\tau \,\mathrm{d}\tau \quad \text{and} \quad \Lambda_{12} = \int_{y=y_0}^{y_0+\Delta y} R^{\Delta y}_{u'u'} \,\mathrm{d}(\Delta y). \tag{6}$$

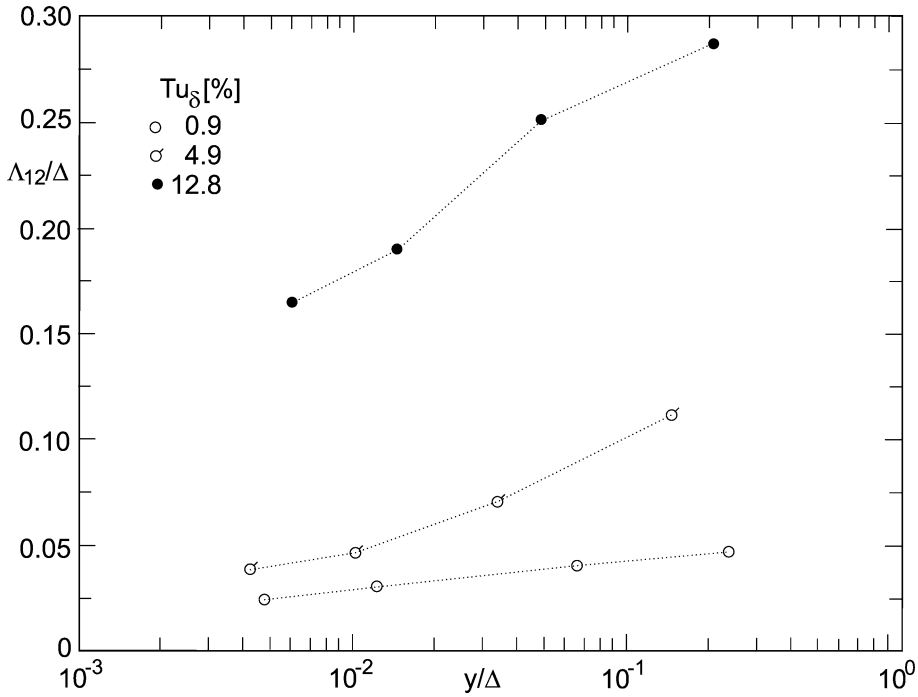

Fig. 22. Distribution of the dimensionless integral length scale Λ_{12}/Δ in outer-law scaling at various FST levels and constant Re_{δ_2}.

The integral length scales $\Lambda_{11} = \Lambda_\tau \cdot \bar{u}$ and Λ_{12} were then plotted in outer-law scaling with the Rotta–Clauser length Δ as the characteristic boundary-layer length scale. The momentum-loss thickness δ_2 would have been another suitable alternative length for normalization.

Figs. 21 and 22 show that integral length scales in both the x- and y-directions with distance from the wall and with increasing turbulence intensity Tu_δ (see also Thole and Bogard [8]). The distributions of Λ_{11} (Fig. 21) have a maximum – approximately at the same value of y/Δ – before they decrease again to the values of the free-stream. For the low turbulence case an increase of Λ_{11}/Δ is observed at the outer edge of the boundary layer which is caused by the shear layer originating at the trailing edge of the turbulence generator upstream. The integral length scale Λ_{12}/Δ in the normal direction to the wall increases by a factor of about two from the inner to the outer region of the boundary layer irrespective of Tu_δ (Fig. 22) and the size of the coherent structures differs by about a factor six between the low and the high turbulence across the boundary layer. This means that both length scales Λ_{11} and Λ_{12} are greatly influenced by the FST.

4. Conclusions

Measurements of mean and fluctuating velocity profiles and of skin friction were performed in an axisymmetric turbulent boundary with zero pressure gradient and free-stream turbulence intensities in the range $1 \leqslant Tu_\delta \leqslant 13\%$ at the first measuring station. The ratio of the integral length scale Λ_{11} in the free-stream to the boundary layer thickness $\delta_{99.5}$ varied between about 0.5 and 2 in the streamwise direction.

The high level of free-stream turbulence was generated by jets injected normal to the flow, the momentum of which was varied to set the turbulence level in the test section, following Thole and Bogard [9]. The data of two often-used techniques to measure skin friction, the Preston tube and the wall hot wire, were compared with those of a direct and absolute method, oil-film interferometry. The results compare well within the uncertainty range of the techniques. At the same Reynolds number Re_{δ_2} the FST increased the skin friction at most by 34% under the present conditions. The skin friction data correlate satisfactorily with the Hancock–Bradshaw–Blair parameter. The increase in skin friction is related to the increased mixing by the FST that penetrates into the boundary layer and which thereby reduces the mean velocity gradient in the outer region, resulting in a fuller profile. The mean velocity profile agrees with the linear law and the logarithmic law in the inner region of the boundary layer independent of Tu_δ. The FST affects significantly the wake parameter and the mean velocity distribution in outer-layer scaling due to Rotta [23]. The distribution of the mean velocity is affected in a similar way as by a mild favourable pressure

gradient. There appears to be convergence of the mean velocity profiles for FST levels above $Tu_\delta \approx 10\%$ as observed by Thole and Bogard [8].

Plotted in inner-law scaling the distributions of the Reynolds normal stress components $\overline{u'^2}/u_\tau^2$ collapse on to each other in the viscous sublayer and the lower part of the buffer layer (note the almost constant Re_{δ_2}) but their peak value increases by about 25% for $Tu_\delta \approx 13\%$ as compared with $Tu_\delta \approx 1\%$.

The Reynolds shear stress profiles extend further out into the outer region of the boundary layer with increasing FST but this does not lead to a higher production of Reynolds normal stress since $\delta\bar{u}/\delta y$ is smaller. In inner-law scaling, as suggested by Rotta [23], the production in the inner layer is practically not affected by the FST.

The effect of the FST on the distributions of the flatness $F_{u'}$ is to eliminate the high values at the edge of the boundary layer, i.e., the boundary layer contour is much smoother. The flatness $F_{u'}$ shows higher values in the vicinity of the wall with increasing FST and this behaviour is confirmed by the equivalent values of $F_{\tau'_w}$ measured at $y^+ \approx 2$ by the wall hot-wire probe. Power spectra E_{11} plotted in Kolmogorov scaling show the expected behaviour in the freestream, different from that in the log-law region where differences due to the FST level are confined to the low wave-number range. The data will be available from the first author in about 2004.

References

[1] P.E. Roach, D.H. Brierly, The influence of a turbulent freestream on zero pressure gradient transitional boundary layer development including the condition test cases T3A and T3B, in: O. Pironneau, et al. (Eds.), Numerical Simulation of Unsteady Flows and Transition to Turbulence, Cambridge University Press, Cambridge, 1989.

[2] M. Kalter, H.-H. Fernholz, The reduction and elimination of a closed reverse-flow region by free-stream turbulence, J. Fluid Mech. 446 (2001) 271–308.

[3] P. Hancock, P. Bradshaw, The effect of free-stream turbulence on turbulent boundary layers, ASME J. Fluids Engng. 105 (1983) 284–289.

[4] P. Hancock, P. Bradshaw, Turbulence structure of a boundary layer beneath a turbulent free stream, J. Fluid Mech. 205 (1989) 45–76.

[5] M. Blair, Influence of free-stream turbulence on turbulent boundary layer heat transfer and mean profile, part I – experimental data, ASME J. Heat Transfer 105 (1983) 33–40.

[6] M. Blair, Influence of free-stream turbulence on turbulent boundary layer heat transfer and mean profile, part II – analysis of results, ASME J. Heat Transfer 105 (1983) 41–47.

[7] K. Thole, D. Bogard, Enhanced heat transfer and shear stress due to high free-stream turbulence, ASME J. Turbomachinery 117 (1995) 418–424.

[8] K. Thole, D. Bogard, High freestream turbulence effects on turbulent boundary layers, ASME J. Fluids Engng. 118 (1996) 276–284.

[9] K. Thole, D. Bogard, J. Whan, Generating high freestream turbulence levels, Expts. Fluids 17 (1994) 375–380.

[10] H.-H. Fernholz, P.J. Finley, The incompressible zero-pressure-gradient turbulent boundary layer: an assessment of the data, Progr. Aerospace Sci. 32 (1996) 245–311.

[11] H.-H. Fernholz, D. Warnack, The effects of a favourable pressure gradient and of the Reynolds number on an incompressible axisymmetric turbulent boundary layer. Pt. 1. The turbulent boundary layer, J. Fluid Mech. 359 (1998) 329–356.

[12] V.C. Patel, Calibration of the Preston tube and limitations on its use in pressure gradients, J. Fluid Mech. 23 (1965) 185–208.

[13] H.-H. Fernholz, G. Janke, M. Schober, P. Wagner, D. Warnack, New developments and applications of skin-friction measuring techniques, Meas. Sci. Technol. 7 (1996) 1396–1409.

[14] B. Stefes, Turbulente Wandgrenzschichten mit und ohne negativen Druckgradienten unter dem Einfluss hoher Turbulenzintensität der Außenströmung, Dissertation, Technische Universität Berlin, 2003.

[15] I.P. Castro, Effects of free-stream turbulence on low Reynolds number boundary layers, Trans. ASME J. Fluids Engng. 106 (1984) 298–306.

[16] D.E. Coles, The turbulent boundary layer in a compressible fluid, Rand Report R-403-PR, 1962.

[17] D.M. Bott, P. Bradshaw, Effect of free-stream turbulence on boundary layer skin friction and heat transfer, AIAA Paper 98-0531, 1998.

[18] H.-H. Fernholz, P.J. Finley, A critical commentary on flow data for two-dimensional compressible turbulent boundary layers, AGARD-AG-253, 1980.

[19] J.M. Österlund, A.V. Johannsson, Dynamic behaviour of hot-wire probes in a turbulent boundary layer, in: Proc. 5th European Turbulence Conference, Sienna, Kluwer, Dordrecht, 1994.

[20] P.R. Spalart, Direct simulation of a turbulent boundary layer up to $Re_\theta = 1410$, J. Fluid Mech. 187 (1988) 61–98.

[21] R.J. Karlsson, T.G. Johansson, LDV measurements of higher order moments of velocity fluctuations in a turbulent boundary layer, in: Laser Anemonetry in Fluid Mechanics, Ladoan-Instituto Superior Tecnico, 1096 L.C., Portugal, 1988.

[22] H. Ueda, J.O. Hinze, Fine-structure turbulence in the wall region of a turbulent boundary layer, J. Fluid Mech. 67 (1975) 125–143.

[23] J.C. Rotta, Turbulent boundary layers in incompressible flow, Progr. Aeronaut. Sci. 2 (1962) 1–221.

[24] J.O. Hinze, Turbulence, McGraw-Hill, New York, 1975.

[25] V.A. Sandborn, R.D. Marshall, Local isotropy in wind tunnel turbulence, Colorado State Univ. Rep. LER 65 AUS-RDM 71, 1965.

[26] D. Warnack, H.-H. Fernholz, The effects of a favourable pressure gradient and of the Reynolds number on an incompressible axisymmetric turbulent boundary layer. Pt. 2. The boundary layer with relaminarization, J. Fluid Mech. 359 (1998) 357–381.